Int. J. Electrochem. Sci., 17 **(2022)** Article Number: 220454, doi: 10.20964/2022.04.45

International Journal of
ELECTROCHEMICAL
SCIENCE
www.electrochemsci.org

Short Communication

Co_3O_4 Nanoflake as High Capacity Anode Materials for Superior Lithium Storage Performance

Yixiao Li

Yongcheng Vocational College, Yongcheng, 476600, China.
E-mail: yixiaoliedu@sina.com

Received: 18 December 2022 / *Accepted:* 3 February 2022 / *Published:* 4 March 2022

Developing new anode materials with high capacity, energy density is of great importance for the application of the lithium-ion batteries. Herein, the lithium storage performance of Co_3O_4 as anode materials is studied by using different morphologies of Co_3O_4 samples, which are obtained at different temperatures. The morphology and structure of the samples are characterized by using SEM, TEM and XRD measurements. The surface area and pore size of the samples are tested by BET analysis. The lithium storage performance of the different Co_3O_4 sample is characterized by discharge/charge, CV and EIS tests. It demonstrates that the as-prepared CONF-1 anode exhibits high initial capacity of 1218 mAh g^{-1} and keep stable capacity of 785 mAh g^{-1} after 300 cycles at high current density of 1 A g^{-1}. The results reported in this work could provide strategies for exploring novel high-performance anode materials from transition metal oxides.

Keywords: Lithium storage; XRD; Capacity; Cycling; Structure.

1. INTRODUCTION

Rechargeable lithium-ion batteries (LIBs) have been widely employed in many fields, such as electric vehicles, mobile phone and portable electronics devices due to their high energy density and long cycle life and environment friendliness [1-5]. Among many components in the LIBs, electrode materials play key role for the electrochemical performance of the LIBs [6, 7]. The graphite anode materials are widely used in the LIBs owing to their low potential, low cost and stable cycling performance [8, 9, 10]. However, the traditional graphite anode materials suffers from low capacity (372 mAh g^{-1}), which inhibits their applications in the high energy density storage systems [11, 12]. Therefore, it is urgent to develop new anode materials with high capacity to meet the requirements of high energy density [13].

Transition metal oxides are promising anode materials for the LIBs due to their high capacities, which is beneficial for the achievements of high energy density [14-16]. Besides, the transition metal

oxides have high catalytic effects, surface area, which could promote the reaction kinetics during the discharging and charging process [17, 18]. Based on these advantages, it is meaningful to develop novel anode materials by using transition metal oxides [19, 20]. However, the huge volume change could lead to structural collapse during the electrochemical cycles [21]. It is known to all that the morphology has great influence on the electrochemical performance of anode materials [22, 23]. Therefore, it is worthy to study the electrochemical performance of different Co_3O_4 morphology samples [24].

In this work, the lithium storage performance of Co_3O_4 as anode materials is studied by using different morphologies of Co_3O_4 samples. The different morphologies of Co_3O_4 samples are prepared by heating the precursor at different temperature (100℃, 200℃). And the samples are labeled as CONF-1 and CONF-2, respectively. The morphology and structure of the samples are characterized by using SEM, TEM and XRD measurements. The surface area and pore size of the samples are tested by BET analysis. The lithium storage performance of the different Co_3O_4 sample is characterized by discharge/charge, CV and EIS tests. It demonstrates that the as-prepared CONF-1 anode exhibits high initial capacity of 1218 mAh g^{-1} and keep stable capacity of 785 mAh g^{-1} after 300 cycles at high current density of 1 A g^{-1}. The results reported in this work could provide strategies for exploring novel high-performance anode materials from transition metal oxides.

2. EXPERIMENTAL

2.1. Preparation of CONF sample

0.6 g $Co(NO_3)_2 \cdot 6H_2O$ was first dissolved in a mixed solution of 80 mL deionized water under stirring for 30 min. Then the precursor solution was transferred in a 100 mL Teflon-line autoclave and kept at 100 °C and 200 °C for 6 h, respectively. As a result, the Co_3O_4 samples were successfully prepared. And the samples are labeled as CONF-1 and CONF-2.

2.2. Materials Characterization

The crystal structure of the samples were analyzed by X-ray diffraction (XRD) patterns (Rigaku D/MAX-2550 PC diffractometer). The microscopic morphology of the samples was observed under scanning electron microscope (FEI Helios Nanolab 600i microscope). High-resolution transmission electron microscope images were collected on a FEI Tecnai microscope. The specific surface area and pore distribution of the samples was tested by Micromeritics ASAP 2460, and calculated by Brunauer-Emmett-Teller (BET) models.

2.3. Electrochemical Measurement

The active material, acetylene black and PVDF are in a mass ratio of 7:2:1 to form uniform slurry. After that, the slurry was uniformly coated on the Cu foil and heated at 120 °C for 12 h.

Lithium foil was used as the counter electrode, 1 mol L^{-1} $LiPF_6$ (EC/DMC = 1:1) was used as the electrolyte, and Celgard 2300 film was used as the separator to assemble the 2032 button cell in glove box with Ar atmosphere for electrochemical measurement. CV and EIS were used to study the electrode using a CHI670E (Shanghai, China). The galvanostatic charge-discharge tests were conducted by a NEWARE BTS-610 (Neware, China).

3. RESULTS AND DISCUSSION

To investigate the morphology of the samples, the scanning electron microscopy was conducted for all samples. As shown in **Fig. 1**a, it can be seen that the as-prepared CONF-1 samples exhibit nanoflake structure with a diameter of 50 nm. The nanoflake samples are uniformly dispersed in the whole SEM images. With increasing the temperature (200℃), the as-prepared CONF-2 samples display similar morphology compared to the CONF-1 samples. As shown in **Fig. 1**b, it can be clearly observed that the nanoflakes of the as-prepared CONF-2 samples are consisted of many small particles. These small particles could provide huge specific surface area to the electrochemical reactions. Furthermore, the crystal structure of the samples was studied by using XRD. As shown in **Fig. 1**c, the typical crystal structure can be clearly observed for the CONF-1 and CONF-2 samples. The diffraction peaks at 32°, 36°, 45°, 61° and 65° are ascribed to the crystal planes of (001), (101), (210), (011) and (022), respectively [25]. This result demonstrates the high purities of the CONF samples. Besides, the inset of **Fig. 1**c shows the TEM image of the CONF-1 samples. It can be observed that the CONF layer is located in the TEM image, which is consistent with the SEM image.

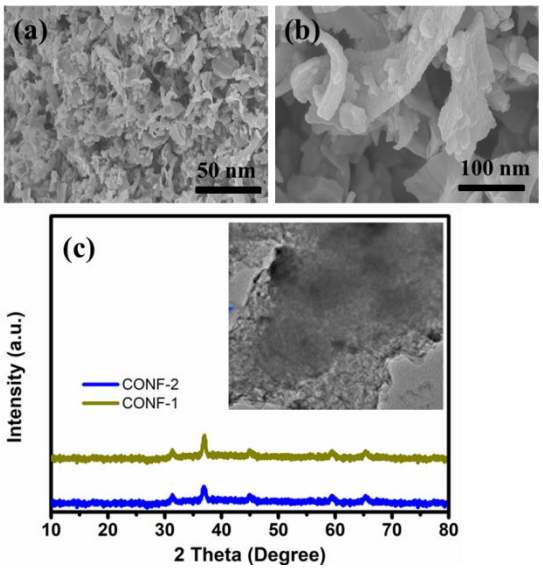

Figure 1. (a) and (b) SEM images of the CONF-1 and CONF-2 samples, respectively. (c) XRD pattern of CONF-1 and CONF-2 samples. The inset is the TEM image of CONF-1.

The pore size and specific surface area of the samples were tested by using N_2 adsorption/desorption test. As shown in **Fig. 2**a, it can be clearly observed that the isotherms of the as-prepared CONF-1 sample correspond to type IV according to IUPAC classification. The mesoporous structure of the CONF-1 samples is beneficial for the transport of the lithium-ion and electrons during the electrochemical cycles. Besides, the specific surface area and pore size of the CONF-1 samples is about 436 m^2 g^{-1} and 10 nm, respectively, which is much higher than the reported Co_3O_4 materials [26]. **Fig. 2b** shows the N_2 adsorption/desorption curves of the CONF-2 sample. Clearly, the as-prepared CONF-2 samples have no mesoporous structure. Besides, the CONF-2 exhibits much smaller specific surface and pore size than the CONF-1 samples. Therefore, it can be inferred that the CONF-1 will display more superior electrochemical performance than the CONF-2 samples.

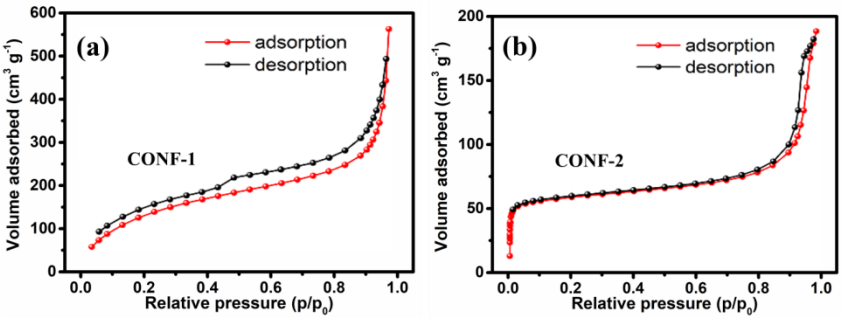

Figure 2. N_2 adsorption/desorption curves of (a) CONF-1 and (b) CONF-2 samples.

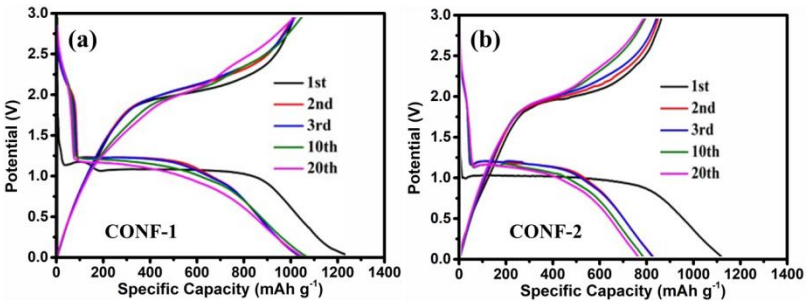

Figure 3. The discharge and charge profiles of (a) CONF-1 and (b) CONF-2 anodes at 0.1 C.

To study the electrochemical performance of the samples, the constant discharge and charge tests were conducted for CONF-1 and CONF-2 samples. The current density is 0.1 C. All cells were tested at room temperature with the same situation. As shown in **Fig. 3**a, the as-prepared CONF-1 electrode exhibits initial high capacity of 1218 mAh g^{-1} at the current density of 0.1 C. Besides, one voltage platform at 1.25 V can be clearly observed during the discharging process. With the increase of the cycle numbers, the CONF-1 electrode still exhibits high capacity of 1013 mAh g^{-1} after 20 cycles, demonstrating stable cycling performance [27]. **Fig. 3**b also exhibits the discharge and charge profiles of the CONF-2 electrode. It can be seen that the CONF-2 electrode shows capacity of 1108 mAh g^{-1},

which is much smaller than the CONF-1 electrode. Moreover, the capacity is only 726 mAh g^{-1} after 20 cycles for the CONF-2 electrode at 0.1 C. The higher capacity of the CONF-1 electrode is attributed to the unique mesoporous structure, which could ensure the rapid lithium transport during the electrochemical reaction [28].

To further investigate the electrochemical mechanism of the CONF-1 electrodes, CV test was conducted for the CONF-1 electrode. As shown in **Fig. 4**a, it shows the initial three cycle CV curves before electrochemical cycles. it can be seen that the as-prepared CONF-1 electrode exhibit typical CV shape with two reduction peaks and one oxidation peak, which is related to the SEI formation and lithium/Co alloy, respectively. **Fig. 4**b is the cycling performance of the CONF-1 and CONF-2 electrode at the current density of 1 A g^{-1} for 300 cycles. It can be clearly observed that the CONF-1 electrode delivered high capacity of of 785 mAh g^{-1} after 300 cycles at high current density of 1 A g^{-1}, demonstrating stable cycling performance. This is attributed to the perfect structure of the CONF-1 electrode, which could promote the lithium-ion and electron transport. However, for the CONF-2 electrode, it suffers from rapid capacity fading during the electrochemical cycles. **Fig. 4**c is the SEM image of the CONF-1 electrode after cycles. It still exhibits perfect morphology compared to the morphology before cycles. Fig. 4d is the CV curve of the CONF-1 electrode after cycles. It can be seen that the CV curves overlap well, indicating superior reversibility.

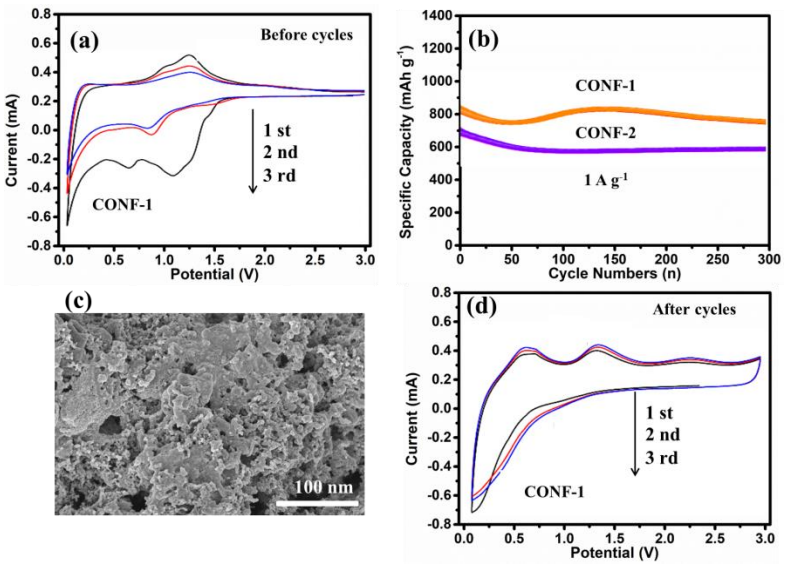

Figure 4. (a) CV curves of CONF-1 before cycles. (b) Cycling performance of CONF-1 and CONF-2 at 1 A g^{-1} after 300 cycles. (c) SEM image of CONF-1 after cycles. (d) CV curves of CONF-1 after cycles.

To clearly demonstrate the advantage of the employment of CONF-1 electrode in the LIBs, schematic illustration was conducted. As shown in **Fig. 5**a, the LIBs used CONF-1 anode exhibits superior lithium storage performance during the electrochemical cycles. Lithium-ions could be easily transferred from the cathode side to the anode side. This is related to the use of the CONF-1 electrode, which could enhance the electrochemical performance. **Fig. 5**b shows the electrochemical impedance

spectra of the CONF-1 and CONF-2 electrode. The EIS is consisted of one semicircle, which represents the charge transfer resistance. Clearly, the as-prepared CONF-1 electrode exhibits much smaller resistance than the CONF-2 electrode. Finally, the long term cycling performance of the CONF-1 electrode is tested at 2 A g^{-1} for 200 cycles. It can be seen that the CONF-1 electrode has capacity of 692 mAh g^{-1} after 200 cycles, indicating the stable cycling performance of the CONF-1 electrode.

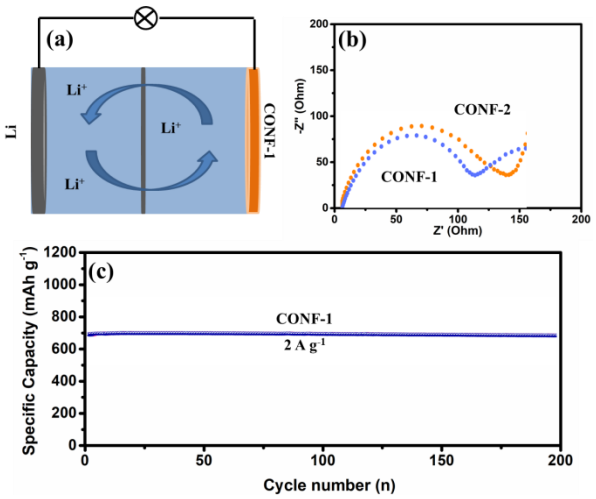

Figure 5. (a) Schematic illustration of the Li//CONF-1 half-cell. (b) EIS of CONF-1 and CONF-2 samples. (c) Long term cycling performance of CONF-1 after 200 cycles.

To further demonstrate the superior electrochemical performance of the CONF-1 anode, a new table was made to compare the electrochemical performance of the anode materials. As listed in Table 1, it can be clearly observed that the as-prepared CONF-1 anode shows high capacity at high current density of 2 A g-1 after 200 cycles, demonstrating the excellent cycling stability. This capacity is much higher than the other similar anode materials reported in literature.

Table 1: The electrochemical performance of CONF-1 and other similar anode materials in LIBs.

Electrode	Current Density	Capacity (mAh/g)	Ref
Fe_7S_8@C	0.1 A g^{-1}	375 (100 cycles)	29
TiO_2	0.5 A g^{-1}	266 (200 cycles)	30
NO/carbon	0.1 A g^{-1}	385 (100 cycles)	31
CONF-1	2 A g^{-1}	692 (200 cycles)	This work

4. CONCLUSION

In summary, the electrochemical performance of Co_3O_4 as anode materials is studied by using different morphologies of Co_3O_4 samples. The different morphologies of Co_3O_4 samples are firstly

prepared by heating the precursor at different temperature (100℃, 200℃). And the samples are labeled as CONF-1 and CONF-2, respectively. Then, the morphology and structure of the samples are characterized by using SEM, TEM and XRD measurements. The surface area and pore size of the samples are tested by BET analysis. The lithium storage performance of the different Co_3O_4 sample is characterized by discharge/charge, CV and EIS tests. It demonstrates that the as-prepared CONF-1 anode exhibits high initial capacity of 1218 mAh g^{-1} and keep stable capacity of 785 mAh g^{-1} after 300 cycles at high current density of 1 A g^{-1}. The results reported in this work could provide strategies for exploring novel high-performance anode materials from transition metal oxides.

References

1. L. Y. Jing, Z. Kong, F. A. Guo, X. H. Liu, A. P. Fu, M. Li, H. L. Li, *J. Alloys Compd*., 881 (2021) 160588.
2. Z. T. Li, J. J. Nie, J. Zhao, J. Wang, X. X. Feng, S. W. Yao, *Mater. Lett*., 285 (2021) 129202.
3. A. R. Mule, D. Narsimulu, A. K. Kakarla, J. S. Yu, *Appl. Surf. Sci*., 551 (2021) 148942.
4. J. W. Wen, L. Xu, J. X. Wang, Y. Xiong, J. J. Ma, C. R. Jiang, L. H. Cao, J. Li, M. Zeng, *J. Power Sources*, 474 (2020) 228491.
5. G. Y. Wang, M. Zhang, Z. P. Deng, X. F. Zhang, L. H. Huo, S. Gao, *Ceram. Int*., 46 (2020) 29033-29040.
6. Y. C. Zhao, C. G. Liu, R. W. Yi, Z. Q. Li, Y. B. Chen, Y. Q. Li, I. Mitrovic, S. Taylor, P. Chalker, L. Yang, C. Z. Zhao, *Electrochim. Acta*, 345 (2020) 136203.
7. Y. G. Liu, H. C. Wan, N. Jiang, W. X. Zhang, H. Z. Zhang, B. D. Chang, Q. Wang, Y. H. Zhang, Z. Y. Wang, S. H. Luo, H. Y. Sun, *Solid State Ionics*, 334 (2019) 117-124.
8. L. Wang, Y. F. Yuan, Y. Q. Zheng, X. T. Zhang, S. M. Yin, S. Y. Guo, *Mater. Lett*., 253 (2019) 5-8.
9. F. Wang, H. Yuan, J. G. Huang, *J. Alloys Compd*., 819 (2020) 153375.
10. M. K. Yu, Y. X. Sun, H. R. Du, C. Wang, W. Li, R. H. Dong, H. X. Sun, B.Y. Geng, *Electrochim. Acta*, 317 (2019) 562-569.
11. J. X. Li, Q. X. Xie, P. Zhao, C. P. Li, *Appl. Surf. Sci*., 504 (2020) 144515.
12. F. C. Zheng, L. Z. Wei, *J. Alloys Compd*., 790 (2019) 955-962.
13. C. W. Zhang, Y. Song, L. B. Xu, F. X. Yin, *Chem. Eng. J*., 380 (2020) 122545.
14. Y. F. Li, Y. Y. Fu, W. B. Liu, Y. H. Song, L. Wang, *J. Alloys Compd*., 784 (2019) 439-446.
15. Y. Xin, X. W. Lan, P. Chang, Y. Q. Huang, L. B. Wang, X. L. Hu, *Appl. Surf. Sci*., 447 (2018) 829-836.
16. J. Y. Cheong, J. H. Chang, S. H. Cho, J. W. Jung, C. H. Kim, K. S. Dae, J. M. Yuk, I. D. Kim, *Electrochim. Acta*, 295 (2019) 7-13.
17. B. Wang, X. Y. Lu, C. W. Tsang, Y. H. Wang, W. K. Au, H. F. Guo, Y. Y. Tang, *Chem. Eng. J*., 338 (2018) 278-286.
18. X. L. Tong, M. Zeng, J. Li, Z. J. Liu, *Appl. Surf. Sci*., 723 (2017) 129-138.
19. Y. F. Lu, X. B. Han, Z. Y. Chu, X. N. Feng, Y. D. Qin, M. G. Ouyang, L. G. Lu, *J. Power Sources*, 513 (2021) 230529.
20. Q. Wang, X. Y. Wu,, H. R. You, H. H. Min, X. K. Xu, J. W. Hao, X. M. Liu, H. Yang, *Appl. Surf. Sci*., 571 (2022) 151194.
21. M. Y. Tian, L. B. Ben, Z. Jin, H. X. Ji, H. L. Yu, W. W. Zhao, X. J. Huang, *Electrochim. Acta*, 396 (2021) 139224.
22. Y. L. Xie, Y. C. Qiu, L. L. Tian, T. F. Liu, X. T. Su, J. Alloys Compd., https://doi.org/10.1016/j.jallcom.2021.162384.
23. R. C. Wang, Q. L. Pan, Y. H. Luo, C. Yan, Z. J. He, J. Mao, K. H. Dai, X. W. Wu,, J. C. Zheng, *J.*

Alloys Compd., 893 (2022) 162089.
24. J. Yu, Y. B. Wei, B. C. Meng, L. J. Wang, L. J. Zhou, N. X. Yang, L. B. Li, *Vacuum*, 193 (2021) 110535.
25. X. F. Chen, X. F. Yang, F. L. Pan, T. T. Zhang, X. Y. Zhu, J. Y. Qiu, M. Li, Y. Mu, H. Ming, *J. Alloys Compd*., 884 (2021) 160945.
26. F. Y. Jiang, Y. Sun, K. X. Zhang, Y. C. Liu, X. Y. Feng, H. F. Xiang, *Electrochim. Acta*, 398 (2021) 139315.
27. N. Cao, Y. L. Zhang, L. L. Chen, W. Chu, Y. G. Huang, Y. Jia, M. Wang, *J. Power Sources*, 483 (2021) 229163.
28. Z. Z. Dang, W. J. Meng, J. Han, D. S. Li, L. Jiang, *J. Alloys Compd*., 891 (2022) 162051.
29. F. Y. Jiang, Q. Wang, R. Du, X. S. Yan, Y. L. Zhou, *Chem. Phys. Lett*., 706 (2018) 273-279.
30. Y. C. Yang, W. Shi, S. J. Liao, R. H. Zhang, S. L. Leng, *J. Alloys Compd*., 746 (2018) 619-625.
31. J. D. Lin, Y. Yuan, Q. Su, A. Q. Pan, S. Dinesh, C. Peng, G. Z. Cao, S. Q. Liang, Electrochim. Acta, 292 (2018) 63-71.